Eur Biophys J (2011) 40:1029–1042
DOI 10.1007/s00249-011-0715-2

ORIGINAL PAPER

Effect of lithium on the electrical properties of polycystin-2 (TRPP2)

María del Rocío Cantero · Horacio F. Cantiello

Received: 1 February 2011 / Revised: 30 April 2011 / Accepted: 18 May 2011 / Published online: 16 June 2011

Abstract Polycystin-2 (PC2, TRPP2) is a TRP-type, non-selective cation channel whose dysfunction is implicated in changes in primary cilium structure and genesis of autosomal dominant polycystic kidney disease (ADPKD). Lithium (Li^+) is a potent pharmaceutical agent whose effect on cell function is largely unknown. In this work, we explored the effect of Li^+ on PC2 channel function. In vitro translated PC2 was studied in a lipid bilayer reconstitution system exposed to different chemical conditions such as Li^+ or K^+ chemical gradients and different symmetrical concentrations of either cation. Li^+ inhibited PC2 function only from the external side, by decreasing the single-channel conductance and modifying the reversal potential consistent with both permeability to and blockage of the channel. When a chemical gradient was imposed, the PC2 single-channel conductance was 144 pS and 107 pS for either K^+ or Li^+, respectively. Data were analysed in terms of the Goldman–Hodgkin–Katz approximation and energy models based on absolute rate theory to understand the mechanism(s) of Li^+ transport and blockage of PC2. The 2S3B model better explained the findings, including saturation, anomalous mole fraction, non-linearity of the current–voltage curves under bi-ionic conditions and concentration dependence of permeability ratios. The data indicate that Li^+ modifies PC2 channel function, whose effect unmasks a high-affinity binding site for this ion, and an intrinsic asymmetry in the pore structure of the channel. The findings provide insights into possible mechanism(s) of Li^+ regulation of ciliary length and dysfunction mediated by this cation.

Keywords TRP channels · Absolute rate theory · Anomalous molar fraction · Primary cilia

Abbreviations

2S3B	Two-site three-barrier model
3S4B	Three-site four-barrier model
ADPKD	Autosomal dominant polycystic kidney disease
ENaC	Epithelial sodium channel
GHK	Goldman–Hodgkin–Katz
GHK_m	Modified Goldman–Hodgkin–Katz
GHK_o	Original Goldman–Hodgkin–Katz
Hepes	4-(2-Hydroxyethyl)-1-piperazineethanesulphonic acid
hST	Human syncytiotrophoblast
PC2	Polycystin-2 (TRPP2)
Perm-selectivity	Permeation selectivity
POPC	Phosphatidyl-choline
POPE	Phosphatidyl-ethanolamine
TM	Transmembrane
TRP	Transient receptor potential
TRPC1	TRP canonical type-1
I/*V*	Current–voltage relationship
V_{rev}	Reversal potential

Electronic supplementary material The online version of this article (doi:10.1007/s00249-011-0715-2) contains supplementary material, which is available to authorized users.

M. R. Cantero · H. F. Cantiello
Cátedra de Biofísica, Facultad de Odontología, UBA, Buenos Aires, Argentina
e-mail: mdrcantero@gmail.com

H. F. Cantiello (✉)
Nephrology Division, Department of Medicine, Massachusetts General Hospital East and Harvard Medical School, Charlestown, MA 02129, USA
e-mail: cantiello@helix.mgh.harvard.edu

Introduction

PC2 is the gene product of *PKD2*, one of the two genes whose mutations cause ADPKD (Mochizuki et al. 1996; Harris and Torres 2009). PC2 was identified as a member of the superfamily of transient receptor potential (TRP) channels with six transmembrane (TM) domains and cytoplasmic amino and carboxy terminals (Fig. 1a; Montell 2001). PC2 was originally associated with non-selective cation channel activity, with slight preference for divalent cations (González-Perrett et al. 2001; Vassilev et al. 2001; Luo et al. 2003). Recently, we determined that PC2 is a structural tetramer (Fig. 1b, see Zhang et al. 2009), with large conductance and multiple subconductance states of identical conductivity (González-Perrett et al. 2001; González-Perrett et al. 2002; Zhang et al. 2009). PC2 also associates with TRP-related channels, such as TRPC1, modifying its conductive and regulation properties (Bai et al. 2008; Zhang et al. 2009). As for other TRP channels, PC2's non-selective cationic activity and selectivity to divalent cations make an important contribution to sensory functions (Cantiello 2003; Voets and Nilius 2003; Delmas 2005; Venkatachalam and Montell 2007). Despite this knowledge of the relationship between molecular architecture and channel properties, ion permeability features of PC2 still await further exploration to uncover correlation between structure and function.

One approach to understand ionic membrane transport, including ion channels, has been the electrodiffusional theory derived by Hodgkin and Katz from the Goldman equation (GHK, Hille 1992). The GHK constant field approximation has been a paradigm to understand ion channel behaviour and explain ionic movement under a number of ionic conditions, particularly those involving ionic gradients (Schultz 1980). Numerical approximations of the Planck–Nernst–Poisson (PNP) electrodiffusional equations have also been successful in fitting a number of current–voltage (*I*/*V*) experimental conditions (Nonner et al. 1999). However, the GHK theory and similar approximations (Schultz 1980; Keener and Sneyd 1992) assume a constant (symmetric) electric field profile that may not necessarily apply to all channels. Other phenomenological approaches have been developed to better understand the molecular steps associated with ion translocation through biological membranes. In such models, the total energy profile for ion translocation can be considered as a series of jumping steps (Glasstone et al. 1941). In contrast to the GHK theory, approach(es) based on energy barriers allow better understanding of phenomena such as multi-occupancy and saturation (Läuger 1973; Hille and Schwarz 1978; Schumaker and Mackinnon 1990). Two energy models have been widely used to explain several features of ion channels: the four-barrier three-site (3S4B, Fig. 1c) model developed by Hille (1975) and the three-barrier two-site (2S3B, Fig. 1d) model contemplating ion–ion interactions (Hille and Schwarz 1978, and variations by Cukierman et al. 1985; Dang and McCleskey 1998; Schumaker and Mackinnon 1990). These

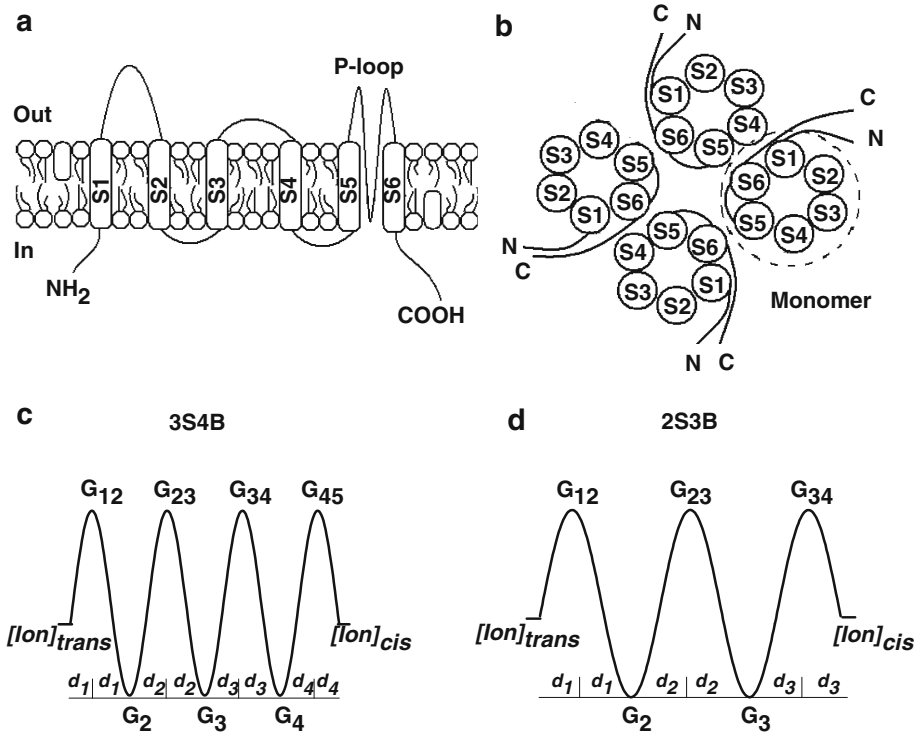

Fig. 1 Schematic representation of PC2 and energy models based on absolute rate theory. **a** PC2 is a TRP-type cation channel with topological features of six TMs (S1–S6), where TMs S5 and S6 form the P-loop associated with the pore. **b** The most likely functional topology of PC2 is a structural tetramer of four homomers that can be partially replaced by other TRP subunits (Zhang et al. 2009). **c** Energy model with three energy valleys G_2, G_3 and G_4, four energy peaks G_{12}, G_{23}, G_{34} and G_{45}, and four partial electrical distances (d_1 to d_4). **d** Energy model with two energy valleys G_2 and G_3, and three energy peaks G_{12}, G_{23} and G_{34}, from *trans* (outside) to *cis* (inside)

energy models have been particularly useful in explaining ionic interactions and blockage of channels such as the blocking effect of Ca^{2+} on rat brain Na^+ channels (French et al. 1994) and Cs^+ on the sarcoplasmic reticulum K^+ channel (Cukierman et al. 1985). The 2S3B model allowed Ismailov et al. (1997) to demonstrate the perm-selectivity of Li^+, Na^+ and K^+ across ENaC. Today little is known, however, about ionic interactions in PC2 and associated TRP channels, which have not been explored to better understand their biophysical properties.

In the present study we explored ionic movement through PC2 with special emphasis on Li^+. Lithium (Li^+) is a potent pharmacological agent that has a profound effect in the treatment of bipolar affective disorder and mania (Machado-Vieira et al. 2009). Recent studies showed that Li^+ causes primary cilium elongation in a number of cultured cell types, including neurons and fibroblasts as well as brain cells, in Li^+-treated animals (Miyoshi et al. 2009). This is rather interesting because the primary cilium is a preferential PC2 location in cells (Nauli et al. 2003; Raychowdhury et al. 2005), where it plays a role in sensory functions (Cantiello 2003; Nauli et al. 2003; Nauli and Zhou 2004). In this work, we assessed the electrical activity of in vitro translated PC2 in a reconstitution lipid bilayer system in the presence of different cationic chemical gradients and increasing symmetrical concentrations of monovalent cations, including Na^+, K^+ and Li^+. We observed that the presence of Li^+ from the extracellular domain (*trans*), but not the cytoplasmic aspect of PC2, reduced the maximal and substate channel conductance and perm-selectivity properties and also changed the reversal potential (V_{rev}) of PC2. This is consistent with both permeability to and a blocking effect of the cation on channel function. Experimental data were analysed in terms of the GHK approximation and different kinetic and energy models based on absolute rate theory (Läuger 1973; Hille 1975; Hille and Schwarz 1978; Schumaker and MacKinnon 1990; French et al. 1994; Ismailov et al. 1997). Although the GHK approximation explained most conditions, a 2S3B energy model better explained ionic saturation and multiple occupancy in PC2. Our data disclosed an asymmetric electric profile in PC2, and a high-affinity Li^+ binding site which may explain our results with clinically relevant low Li^+ concentrations (Timmer and Sands 1999).

Methods

In vitro transcription/translation of PC2

In vitro translated PC2 was prepared as previously reported (Xu et al. 2003; Zhang et al. 2009). Briefly, the plasmid pGEM-PKD2 was transcribed and translated in vitro with the TnT-T7 coupled reticulocyte lysate system (Promega Corp., Wisconsin, USA) in the presence or absence of microsomal membranes. In vitro translated PC2 was sonicated and/or dialyzed with lipids to form PC2-containing liposomes for ion channel reconstitution.

Ion channel reconstitution

Lipid bilayers were formed with a mixture of synthetic phospholipids (Avanti Polar Lipids, Birmingham, AL) in *n*-decane as previously reported (Xu et al. 2003; Zhang et al. 2009). The lipid mixture was made of a 7:3 ratio of 1-palmitoyl-2-oleoyl phosphatidyl-choline (POPC) and phosphatidyl-ethanolamine (POPE). The lipid solution (20–25 mg/ml) in *n*-decane was spread in the aperture of a polystyrene cuvette (CP13-150) of a bilayer chamber (model BCH-13; Warner Instruments Corp., Holliston, MA, USA).

Solutions

All experiments were initiated with one side of the lipid bilayer chamber bathed with a solution containing KCl 150 (mM), Ca^{2+} (10–15 μM) and HEPES (10 mM), adjusted to pH 7.40 using 3 M KOH. The opposite side of the chamber was bathed with a similar solution except for the presence of lower KCl (15 mM). A KCl chemical gradient was thus established, such that no osmotic compensation was present in the reconstitution chamber. For symmetrical cation concentrations, stock solutions of KCl (3 M), NaCl (2 M) and LiCl (2.5 M) were prepared and added to either side of the reconstitution chamber.

Data acquisition and analysis

Electrical signals were obtained using a PC501-A patch clamp amplifier (Warner Instruments, Hamden, CT) with a 10 GΩ feedback resistor. Output (voltage) signals were low-pass filtered at 700 Hz (3 dB) with an eight-pole, Bessel-type filter (Frequency Devices, Haverhill, MA). Signals were acquired using pCLAMP 6.0.2 (Axon Instruments, Foster City, CA) and displayed on an oscilloscope. Single-channel current traces were further filtered for display purposes only. Unless otherwise stated, pCLAMP 10.2 was used for data analysis.

Calculation of cationic perm-selectivity ratios

The perm-selectivity ratio of PC2 for monovalent cations was calculated from the ratio P_S/P_K for fitted values obtained using the Goldman–Hodgkin–Katz (GHK_o) "current" equation (Hille 1992) (see Electronic Supplementary Material, ESM, Eq. S1). Whenever indicated, the GHK_o equation was modified to better fit the experimental data (GHK_m, Eq. S2) by addition of a constant *r* multiplying the

voltage factor (Mackey and McNeel 1971, see ESM). Whenever the experimental data V_{rev} was calculated, values were obtained as the intersection of the linear relationship between data points near zero current and the voltage.

Kinetic modelling of data in symmetrical solutions

Single-channel conductances (g) obtained as a function of ionic activity (γ_i) for ion i (K^+, Na^+ or Li^+) were fitted with a Hill-type kinetic model obeying the function

$$g = \frac{(\gamma_i)^n}{(\gamma_i)^n + (K_D)^n}, \quad (1)$$

where n is the number of binding sites and K_D is the apparent dissociation constant of the complex. Whenever data were plotted as a function of γ_i, the activity coefficient for each ion was obtained from Lide (2009–2010). To calculate K_D, whenever strong negative allosteric interactions occurred, the non-simplified form for two sites with different affinities was used (Segel 1975; see ESM, Eq. S3).

Models based on Eyring rate theory

Eyring absolute rate theory (Glasstone et al. 1941; Eyring et al. 1949; Zwolinski et al. 1949) describes any rate process in terms of elementary jumps over energy barriers. Different models based on this theory have been described to explain ion movement across channels.

(a) *Single-vacancy model*: Single-vacancy conduction is one of the two limits of discrete state models, with the single-ion model being the other limit (Läuger 1973; see ESM for more details). The single-vacancy model describes the relationship between g and increasing ionic activity (γ_i) following a hyperbolic equation (Schumaker and MacKinnon 1990) of the type

$$g = \frac{z^2 e^2}{k_B T}\left(\frac{\gamma_S}{A + B\gamma_S + C\gamma_S^2}\right), \quad (2)$$

where k_B is the Boltzmann constant, z is the valence of the ion, e is the elementary charge and T is absolute temperature. The coefficients A, B and C in Eq. 2 relate to the rate constants for ion entry and exit from the channel, and for ion hopping between binding sites, respectively (see ESM for more details).

(b) *Multi-barrier energy models*: To calculate the free energy profile for ions within the channel pore, currents through PC2 were fitted with a 3S4B model (Fig. 1c, see ESM for more details; Hille 1975), described by Eq. 3

$$I = z_i F \frac{Q\left([S^+]_{cis}\exp(V) - [S^+]_{trans}\right)}{\exp[G_{34} + (d_1 + d_2)V] + \exp[G_{23} + (d_1 - d_3)V] + \exp[G_{12} - (d_2 + d_3)V] + \exp[G_{45} + (d_3 - d_1)V]}, \quad (3)$$

where Q is the frequency constant, G_{12}, G_{23}, G_{34} and G_{45} are the peak energies (Fig. 1c), d_1 to d_4 are electrical distances and V is the reduced voltage ($V = V_h F/RT$) (Hille 1975). Currents through PC2 were also fitted with a 2S3B model (Fig. 1d, Hille and Schwarz 1978, see ESM) that considers interactions between ions by introducing the parameter $A = F_{out}/F_{in}$, where F_{in} and F_{out} are the repulsion factors from the internal and external sides, respectively. Current–voltage experimental data were fitted, for middle and high activity ranges, following Eqs. S7 and S8 (see ESM, Hille and Schwarz 1978).

Statistics

Sigmaplot 11 software was used to conduct statistical analysis and produce graphics (Jandel Scientific, Corte Madera, CA). The criterion to evaluate goodness of fit was based on iterative conversion using the Marquardt–Levenberg algorithm to find the coefficients of the independent variable(s), based on minimizing the sum of squared differences between the observed values and those predicted for the dependent variable. Average data values are expressed as mean ± standard error of the mean (SEM) (n) under each condition, where n represents the number of experiments analysed. Comparisons between two groups of data were conducted by Student's t test, with statistical significance for $P < 0.05$.

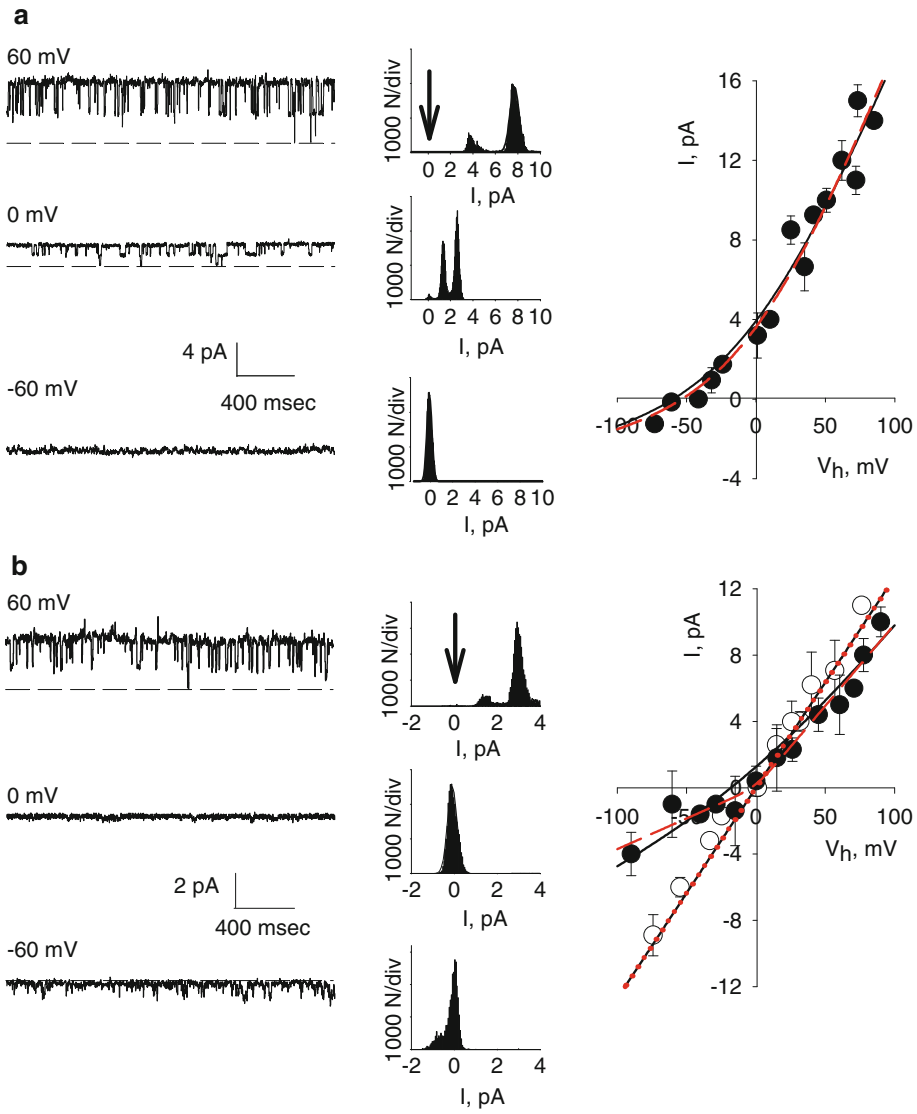

Fig. 2 Single-channel currents of PC2 in asymmetrical K^+. Holding potentials are indicated on top of each trace. **a** Representative single-channel traces (*left*) of in vitro translated PC2 in a "forward" KCl chemical gradient, all-point histograms (*middle*) and *I/V* relationship (*right*). **b** Representative single-channel traces (*left*) of in vitro translated PC2 after addition of LiCl *trans* (135 mM), all-point histograms from traces on the left (*middle*) and *I/V* relationship (*right*) in symmetrical KCl (150 mM, *open circles*) and in the presence of a "forward" KCl chemical gradient after addition of 135 mM LiCl to the *trans* side (*filled circles*, $n = 4$) (*middle*). All experimental data (mean ± SEM, $n = 6$) were fitted with either GHK_o (Eq. S1, *black line*) or GHK_m (Eq. S2, *red line*)

Results

Conductance properties of PC2 in the presence of KCl chemical gradient: effect of Li^+

The first aim of this study was to determine the effect of Li^+ on the conductive properties of in vitro translated PC2 following incorporation in a lipid bilayer system in the presence of a K^+ chemical gradient (150 mM *cis*, 15 mM *trans*) (Fig. 2a). Single-channel currents exhibited strong cation permeability as indicated by the fitting of experimental data to the GHK_o equation (Eq. S1), which rendered a reversal potential of $V_{rev} = -59.5 \pm 1.4$ mV and a maximal conductance of 144 ± 10.1 pS ($n = 6$, Fig. 2a right, Table 1) as previously reported (González-Perrett et al. 2001). Addition of either KCl or LiCl to the *trans* side to eliminate the cationic chemical gradient (135 mM) resulted in a decrease of g, as expected following the GHK prediction (Fig. 2b right). For symmetrical K^+, g was 127 ± 2.5 pS ($n = 4$) and V_{rev} was 0 mV (Fig. 2b, open symbols). Addition of 135 mM LiCl to the *trans* chamber, however, decreased the maximal as well as substate channel conductance (Figs. 2b, 3) in positive potentials (Fig. 2b left) as compared with symmetrical K^+ (82.4 ± 8.5 pS versus 127 ± 2.5 pS, $P < 0.05$). However, the decrease in maximal (Fig. 2b right, filled symbols) and substate channel (Fig. 3) conductance was more evident at negative holding potentials, where experimental data rendered V_{rev} of 0.0 ± 0.2 mV. Fitting of experimental data with the GHK_o equation (Eq. S1) was poor since the theoretical V_{rev} was −16.8 ± 0.9 mV (Fig. 2b, black line). To improve the fitting, data were further evaluated with a modified GHK_m equation (Eq. S2, see ESM for details) rendering a g of 97.8 ± 1.2 and a V_{rev} of 0.78 ± 0.31 mV,

Table 1 Comparison of electrical parameters obtained from fitting current–voltage relationships with the GHK, 2S3B and 3S4B models

	GHK_o		GHK_m		3S4B		2S3B	
	g (pS)	V_{rev} (mV)	g (pS)	V_{rev} (mV)	g (pS)	V_{rev} (mV)	g (pS)	V_{rev} (mV)
K_{cis}, 150 K_{trans}, 15	144	−59.5	144	−54.7	136	−56.1	145	−54.4
Li_{cis}, 150 Li_{trans}, 15	107	−59.0	109	−57.0	89.4	−55.6	116	−54.7
K_{cis}, 15 K_{trans}, 150	79.7	59.3	105	36.1	140	55.8	136	55.1
K_{cis}, 150 K_{trans}, 150	127	0	127	0	131	0	112	0
K_{cis}, 150 K_{trans}, 15 Li_{trans}, 135	82.4	−16.8	97.8* 37.8$^+$	0.78	106	3.2	107.0* 67.0$^+$	−9.5
K_{cis}, 15 K_{trans}, 150 Li_{cis}, 135	115	0	115	0	112	−7.9	108	0

The table presents the channel conductance and the reversal potentials obtained from data fitting of *I/V* curves under various ionic conditions

* Positive holding potentials

$^+$ Negative holding potentials

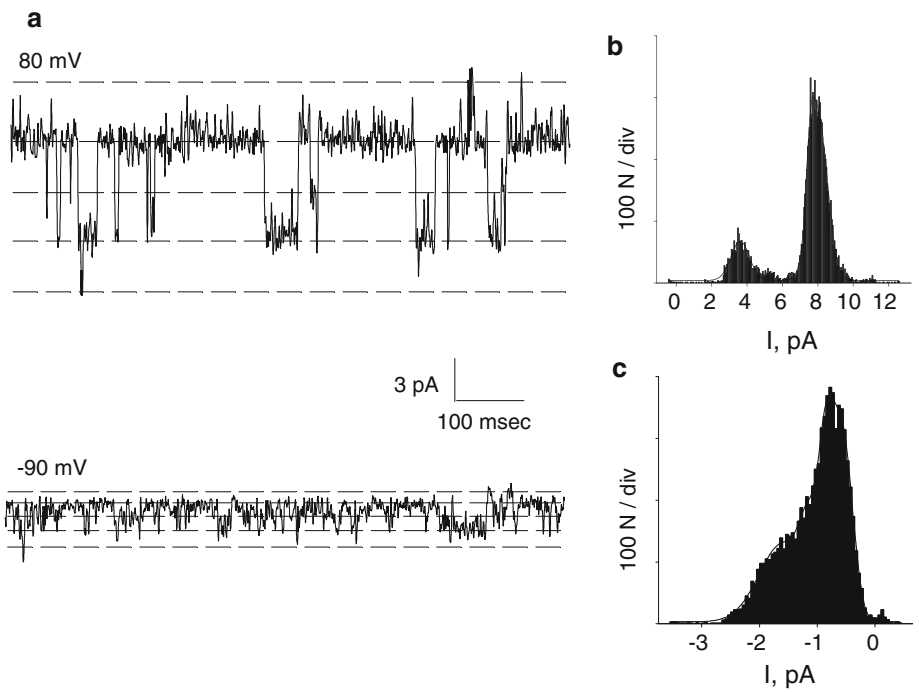

Fig. 3 Conductance substates of PC2 channel in the presence of Li^+. **a** Representative single-channel traces of in vitro translated PC2 in a "forward" KCl chemical gradient after addition of Li^+ (135 mM) to the *trans* compartment at 80 mV (K^+ movement, *top*) and −90 mV (Li^+ movement, *bottom*), respectively. **b** All-point histograms from traces at 80 and at −90 mV. Data are representative of four experiments

thus closer to the experimental data (Fig. 2b right, red line). The perm-selectivity (P_{Li}/P_K) ratios calculated from permeability coefficients P_i obtained by fitting the experimental data under bi-ionic conditions to either the GHK_o or GHK_m equations were 0.82 and 0.30, respectively (Table 2). Thus, the modified GHK predicts a much lower Li^+ permeability.

Conductance properties of PC2 in the presence of a "reversed" KCl chemical gradient

To further explore whether there was sidedness to the effect of Li^+ on PC2 function, the channel was first reconstituted in the presence of a "reverse" KCl chemical gradient (15 mM *cis*, 150 mM *trans*). Under these

Table 2 Comparison of electrical parameters under different ionic conditions

Mono-ionic conditions	K^+ 150/15		K^+ 150/150		K^+ 15/150		Li^+ 150/15	
	GHK_o	GHK_m	GHK_o	GHK_m	GHK_o	GHK_m	GHK_o	GHK_m
g (pS)	144	144	127	127	79.7	105	107	109
P_i (m s^{-1}) [$\times 10^{-7}$]	3.01	3.10	2.28	2.20	1.99	1.99	2.20	2.0

Bi-ionic conditions	K^+, 150/15 Li^+, 0/135		K^+, 15/150 Li^+, 135/0	
	GHK_o	GHK_m	GHK_o	GHK_m
g (pS)	82.4	97.8	115	115
P_K (m s^{-1}) [$\times 10^{-7}$]	1.5	1.76	2.06	2.06
P_{Li} (m s^{-1}) [$\times 10^{-7}$]	1.25	0.54	2.06	2.06

The table contains the single-channel conductance (g) and permeability coefficient (P_i) for the ion, obtained from fits of data to the GHK equations under several ionic conditions

conditions, fitting of experimental data with the GHK_o equation (Eq. S1) rendered $V_{rev} = 59.3 \pm 1.3$ mV ($n = 4$, Fig. 4a, Table 1) and g of 79.7 ± 1.2 pS (Fig. 4a), which was much lower than that observed with the "forward" gradient. Fitting was again improved with the GHK_m (Eq. S2), except for the range of voltages close to V_{rev} (Fig. 4a, Table 1), which was lower than that observed either with the experimental data or by fitting the data with GHK_o. Under these conditions, addition of LiCl to the *cis* side to reach final cationic concentration of 150 mM resulted in an *I/V* curve similar to that observed in symmetrical KCl (Fig. 4b, filled versus open symbols). Under symmetrical conditions, both GHK_o and GHK_m rendered similar good fits for either mono-ionic K^+ or bi-ionic K^+/Li^+. The P_{Li}/P_K ratio obtained under bi-ionic conditions ($V_{rev} = 0$ mV) was 1.0, indicating that Li^+ permeates as well as K^+ when added from the *cis* compartment. This is in contrast to the observation in the presence of Li^+ *trans*, where there was a deviation from linearity in the *I/V* curve, particularly at negative holding potentials (Fig. 2b right, filled symbols). Thus, Li^+ exerts a blocking effect only from the *trans* side.

PC2 conductance in the presence of LiCl chemical gradient

To evaluate Li^+ permeation in the absence of K^+, PC2 channel activity was determined in the presence of Li^+ "forward" chemical gradient (150 mM *cis*, 15 mM *trans*, Fig. 4c). In vitro translated PC2 exhibited the expected cation permeability with V_{rev} of −59.0 ± 1.4 mV ($n = 3$) and g of 107 ± 3.5 pS (Fig. 4c), as assessed by fitting of the experimental data to the GHK_o equation (Eq. S1). These data confirmed an electrodiffusional GHK response similar to but 74.3% lower than that observed in the presence of a "forward" K^+ chemical gradient (Fig. 4c, black line versus dotted line, and Fig. 2a right). The ratio of the fitted GHK_o equations for both K^+ and Li^+ "forward" gradients rendered a constant P_{Li}/P_K perm-selectivity ratio of 0.74 for all voltages.

Conductance properties of PC2 for a single permeant ion

To further assess the issue of ionic interactions within the PC2 channel pore, its activity was determined in the presence of symmetrically increased salt concentration in both bathing solutions. This experimental condition resulted in a saturating function of g versus γ_i for the three cations tested K^+, Na^+ and Li^+ (Fig. 5). A symmetrical increase in KCl for γ_i in the range 10 mM to 1.0 M increased g from 31.8 ± 14.9 pS to 200 ± 14.4 pS ($n = 9$, Fig. 5a, d), respectively. Further increase in γ_K decreased g to 175 ± 10.1 pS (1.4 M KCl, $P < 0.05$). A similar effect was observed in the presence of NaCl. A symmetrical increase in NaCl from 10 mM to 0.85 M increased g from 33.1 ± 11.0 to 163 ± 10.0 pS ($n = 8$, Fig. 5b, e), which decreased to 141 ± 13.0 pS at higher concentrations ($P < 0.05$, Fig. 5b, e). In the case of Li^+, the maximal g was 67.4 ± 6.9 pS ($n = 10$, Fig. 5c, f) at activity of approximately 1–1.5 M LiCl with no evidence of decrease. The experimental data were fitted using a Hill-type equation (Eq. 1). The best fit for K^+ was obtained with $n = 2.07 \pm 0.15$ and K_D of 200 ± 87 mM (Fig. 5a). The NaCl and LiCl data rendered $n = 1 \pm 0.31$ and K_D of 170 ± 38.7 mM (Fig. 5b) for Na^+, and $n = 0.67 \pm 0.13$ and $K_D = 100 \pm 98$ mM (Fig. 5c) for Li^+. The large dispersion of fitted data for the Li^+ condition suggested a

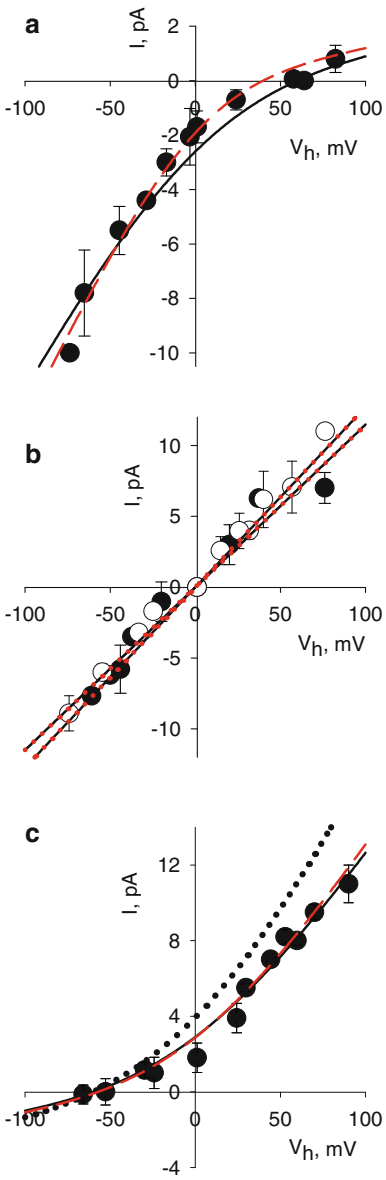

Fig. 4 Current–voltage relationships of PC2. All experimental data were fitted with GHK_o (Eq. S1, *black line*) and with GHK_m current equations (*red line*). **a** *I/V* relationship in the presence of a "reverse" KCl chemical gradient. Data (*filled symbols*) are mean ± SEM ($n = 4$). **b** *I/V* relationship in symmetrical KCl (150 mM, *open circles*) and in the presence of a "reverse" KCl chemical gradient after addition of 135 mM LiCl to the *cis* side (*filled circles*, $n = 3$). **c** *I/V* relationship in the presence of a LiCl chemical gradient ($n = 3$). The *dotted line* represents the GHK_o fit of single-channel data in KCl "forward" chemical gradient, for comparison

different binding interaction, most likely negative cooperation between the single salt ions within the channel pore. Multiple occupancy within the PC2 channel is supported by the bending-down shape of g as a function of γ_i for either ion. For this reason the experimental data were also fitted using the single-vacancy model (Eq. 2; Schumaker and MacKinnon 1990; see "Methods" and ESM). Data were fitted to Eq. 2 for $n = 2$–4 for K^+ and Na^+ and $n = 1$–4 for Li^+ (Fig. 5d–f; Table 3), which rendered K_D of 250 mM for K^+, 200 mM for Na^+ and 100 mM for Li^+. The fitted A, B and C constants (Eq. 2; Table 3), however, suggested much stronger linear (B) and weakly quadratic (C) factors for Li^+ compared with either K^+ or Na^+. Fitting of the data to the single-vacancy model predicted, with some deviation, the strong reduction in g as a function of γ_i only for K^+ (Fig. 5d), considering two and four interacting sites. Moreover, Li^+ data were well fitted assuming only one interacting site, as indicated by the large B factor (Table 3). To further explore the existence of a second interacting site in the Li^+ data, the changes in g, plotted as a function of symmetrical ionic activity, were fitted to Eq. S3 (Fig. 5c, inset), which were consistent with a strong negative allosteric interaction. The experimental data were best fitted with two K_D values of 19 mM and 1 M for the first and second binding sites, respectively. These findings suggested that the high-affinity binding site may represent the inhibitory constant for Li^+ interaction within the pore. A detailed inspection of the changes of $\gamma_i g^{-1}$ versus γ_i can be found in Fig. S2 (left). This shows that most of the K^+ experimental data in the range 10–600 mM departed slightly from the single-vacancy model, which should follow a quadratic function (Schumaker and MacKinnon 1990). Stronger deviations were also found for the Na^+ and Li^+ data, respectively. Whenever the relationship g/γ_i versus γ_i was plotted for each ion (Fig. S2 right), two regimes of permeation were observed, suggesting a faster change in permeability at lower ionic activity. This faster mode is less evident in the Li^+ data (Fig. S2f).

Fitting of experimental data to energy models

To better explain the ionic interactions within the channel pore, PC2 ionic currents were fitted with absolute rate theory (Eyring et al. 1949) by using 3S4B and 2S3B models (see "Methods", Fig. 1, Eqs. 3, S7 and S8). The data in Fig. 6a–e indicate that the experimental currents under all conditions were satisfactorily fitted with both energy models (Table 1). The data for both K^+ and Li^+ forward gradients, however, showed better fits with the 3S4B model considering that most experimental data points are exactly fitted by the theoretical curve (Fig. 6a, e). However, the goodness of fit was not statistically different for either model. For this reason and because the 2S3B model is the only one that includes ion–ion interactions (Fig. 5), we further explored this model. The P_{Li}/P_K perm-selectivity ratio obtained from the fitted curves for the 2S3B was a constant value of 0.71, thus voltage independent, in agreement with the GHK_o model (Fig. 6f). The perm-selectivity ratio calculated from fitting with the 3S4B model, however, was lower and showed slight voltage

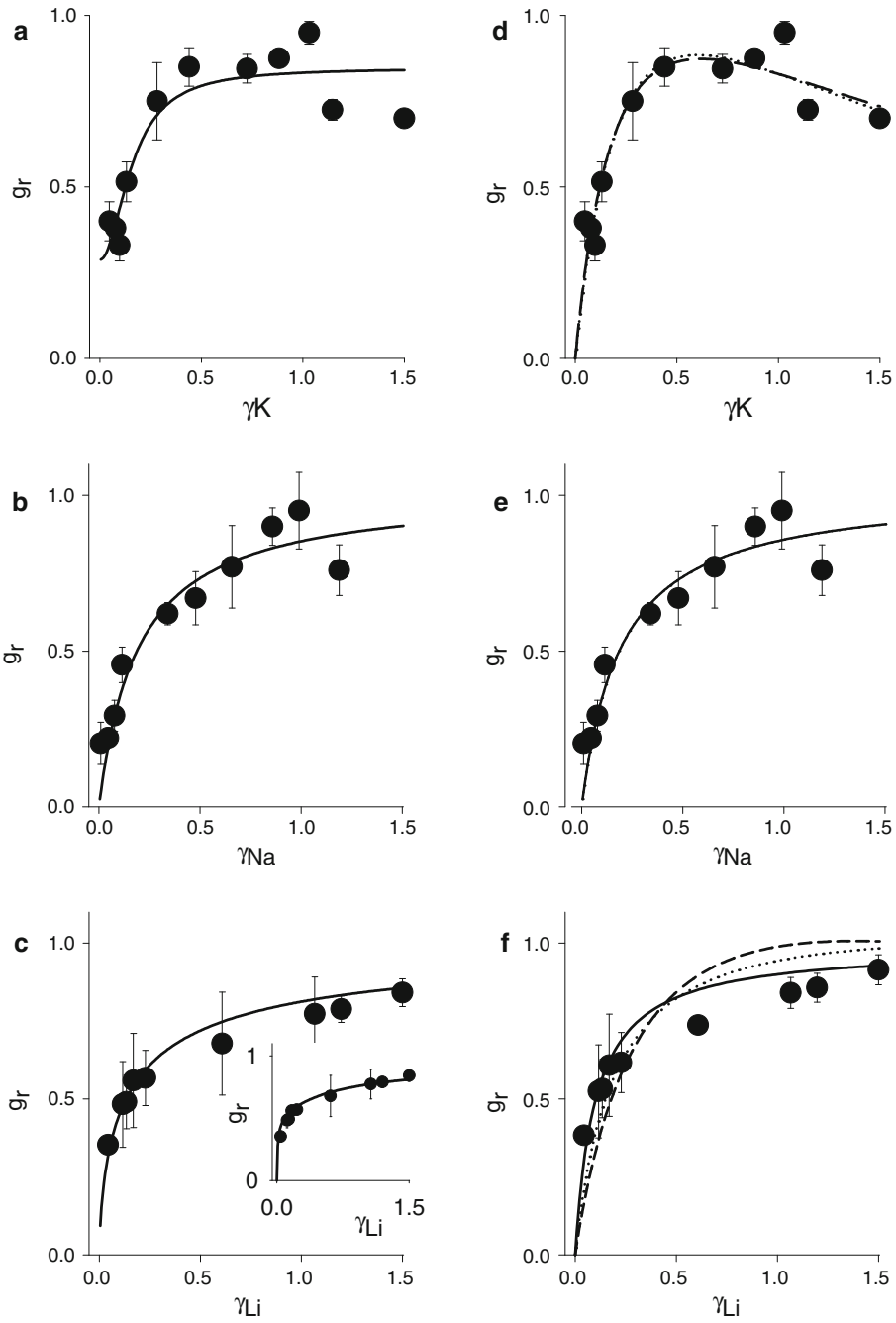

Fig. 5 Dependence of PC2 channel conductance on ionic activity. Relationship between g and γ_i for either K^+ (**a**, **d**), Na^+ (**b**, **e**) or Li^+ (**c**, **f**). Experimental data are mean ± SEM of 8, 10 and 9 experiments, respectively. Data were fitted either with a Hill-type kinetic equation (*left panels*) or with the single-vacancy model (*right panels*). *Panel c inset* (see ESM) was fitted with Eq. S3

dependence between 0.51 and 0.55 (Fig. 6f). The energy profile obtained by the best fit of all experimental data with the 2S3B model is shown in Fig. 7. This model shows that Li^+ has deeper valley energies ($G_2 = -8.0$ kT versus -5.6 kT, and $G_3 = -6.3$ kT versus -4.3 kT, for Li^+ and K^+, respectively; Fig. 7). Table S1 summarizes the energy parameters obtained with the 2S3B model. The ΔG_2 and ΔG_3 obtained for K^+ and Li^+, respectively, indicate differences of 2.4 kT and 2.0 kT, respectively, corresponding to the relationship $g_{Li}/g_K = 0.74$. The valley energies predicted a K_D for the first binding site calculated from Eq. S6 of 18.7 mM for Li^+ and 205 mM for K^+, respectively. The results are consistent with the experimental data of Fig. 5 (K_D calculated with Eq. S5).

Effect of low Li^+ concentrations on PC2 channel function

The energy model and calculated K_D indicated a much higher affinity and stronger interaction of Li^+ than K^+

Table 3 Kinetic parameters obtained from the single-vacancy and the Hill models

Ion	Single-vacancy model									Hill-type equation		
	a (s^{-1} M^{-1}) [$\times 10^8$]	b (s^{-1}) [$\times 10^8$]	k (s^{-1}) [$\times 10^8$]	n	K_D^a (M)	A (Ms) [$\times 10^{-8}$]	B (s) [$\times 10^{-8}$]	C (s M^{-1}) [$\times 10^{-8}$]	R	n	K_D^a (M)	R
K^+	4.70	1.20	1.42	2	0.25	8.51	3.08	2.76	0.93	2	0.20	0.90
	10.1	2.52	4.81	4	0.25	0.81	1.21	2.50	0.94			
Na^+	2.36	0.48	2.15	2	0.20	1.54	2.54	2.28	0.92	1	0.17	0.91
	4.60	1.09	5.77	4	0.23	1.74	2.99	2.19	0.92			
Li^+	1.22	0.13	1×10^{-8}	1	0.11	1.64	15.4	0	0.86	0.67	0.10	0.96
	1.44	0.14	22	2	0.10	2.78	14.8	0.47	0.89			
	2.07	0.21	15	4	0.10	3.86	10.3	1.97	0.77			

This table contains the kinetic parameters that allowed calculation of the dissociation constants, including ion entry (a) and exit (b) from a binding site and ion hopping between sites (k) obtained by the single-vacancy model. The table also contains the dissociation constants and the number of binding sites obtained from the Hill-type kinetic model

[a] K_D is calculated using Eqs. 1 and S5

within the pore, which would explain its blocking effect on channel function. Clinically relevant external Li^+ concentrations in the range 1–10 mM (Timmer and Sands 1999) induced flickering and a reduction in PC2 channel activity (Fig. 8), such that the mean single-channel current decreased (with respect to control activity, 100%) on average to 87 ± 8% ($n = 6$) and 79 ± 3% ($n = 3$) after addition of Li^+ *trans* at 1 and 10 mM, respectively ($P < 0.001$). This suggests a potentially blocking effect of this ion on PC2 channel at therapeutically relevant concentrations.

Discussion

The present study was conducted to assess the interaction between Li^+ and the TRP-type channel PC2. In vitro translated PC2 in the presence of either K^+ or Li^+ "forward" chemical gradients (150 mM *cis*, 15 mM *trans*) showed well-behaved characteristic cationic selectivity, which followed GHK electrodiffusional behaviour. The g and perm-selectivity properties obtained from the *I/V* ratios for respective ions under mono-ionic conditions indicated 25% lower permeability for Li^+ compared with K^+, which remained constant throughout the entire voltage range tested (Table 2). The GHK_o theory (Eq. S1), which provides an analytical solution to the electrodiffusional problem through the channel, rests on the idea of a constant field approximation (Hille 1992). It is however evident that the experimental data under some of the experimental conditions departed from this behaviour, suggesting that either non-linearity in the electrical field or multiple ionic interactions or both might be present in the pore. The "reverse" K^+ chemical gradient, for example, rendered 45% lower g with respect to that under "forward" conditions. Interestingly, these data were better fitted with a modified GHK_m equation (Eq. S2), where the voltage component was modified by a factor r multiplying the holding potential (see ESM). This suggests a non-constant field (or multi-occupancy, Hodgkin and Keynes 1955; Hille and Schwarz 1978) inside the channel that is made evident under "reverse" conditions (Fig. S1), rendering a 25% higher g than that obtained with the GHK_o equation (Table 2). Fitting of the data obtained after dissipation of the K^+ gradient by addition of Li^+ *trans* was better approximated with the GHK_m equation (Fig. 2b right, Table 2). However, addition of Li^+ *cis* (135 mM) to dissipate the cationic gradient under "reverse" conditions rendered identical fits for the GHK_o and GHK_m equations (Table 2). As expected for the sidedness of the Li^+ effect, these results suggest that Li^+ only inhibits PC2 channel function from the external side of the channel, masking the non-constant field and the asymmetry of the pore.

To further assess multiple ionic interactions within the channel pore, monovalent salt concentrations were symmetrically increased in both bathing solutions. This allowed exploration of the changes in g as a function of γ_i, which resulted in saturation of g (with a maximum above 1–1.5 M) for all three cations tested, i.e. K^+, Na^+ and Li^+. This finding, which is consistent with multi-ion occupancy in PC2, would be in agreement with previous findings for other channels (Hladky and Haydon 1972; Urban et al. 1978; Urban and Hladky 1979). The K_D for Na^+ and Li^+ (Table 3) indicated 118–200% higher affinities compared with K^+. Multi-occupancy for both K^+ and Na^+ was also suggested by the bending down of the changes in g versus γ_i, which was only missing in the case of Li^+ (Schumaker and MacKinnon 1990). This is in agreement with Ismailov et al.'s (1997) results for Na^+ and Li^+ interactions with reconstituted ENaC. The difference in n obtained from the

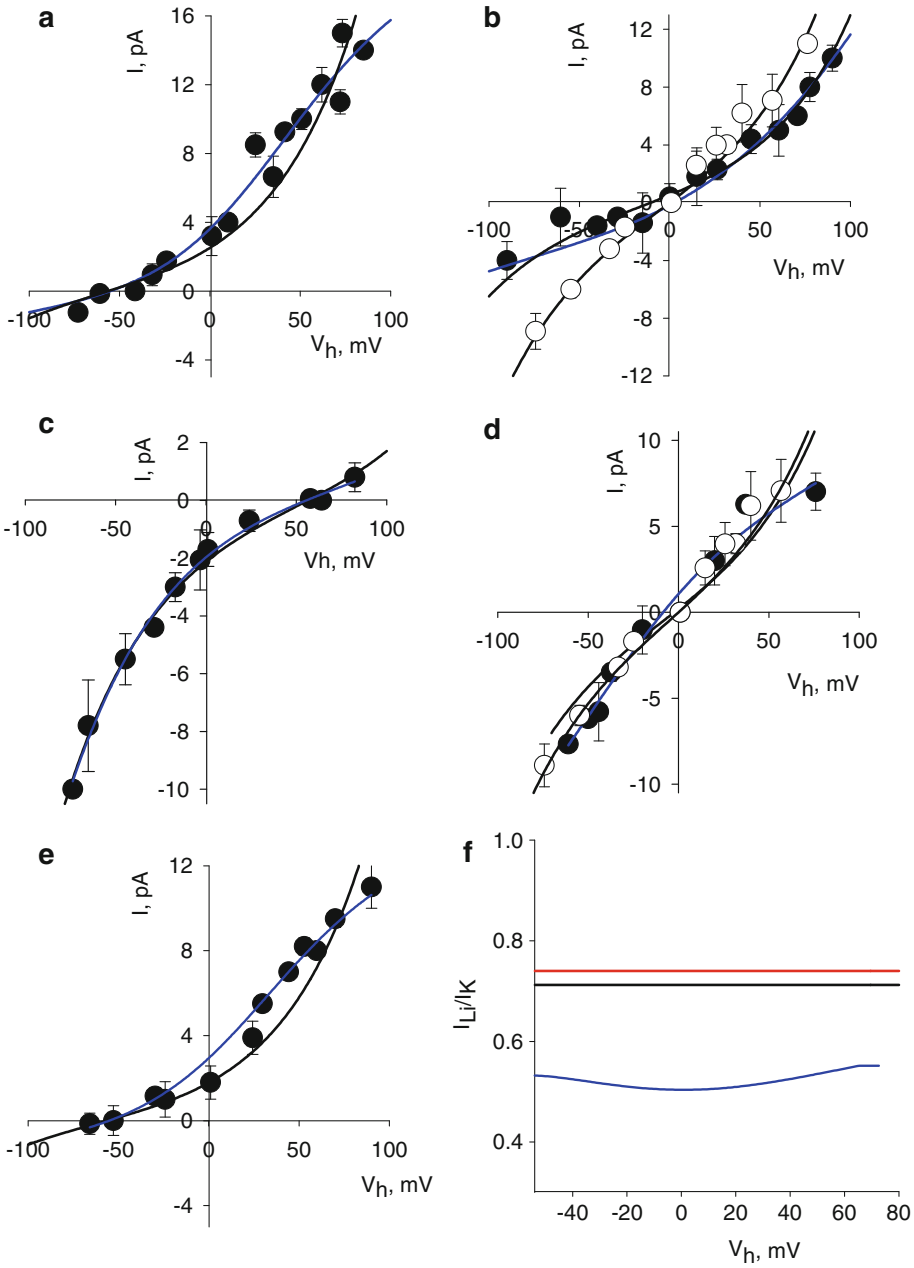

Fig. 6 Fits of *I/V* relationships to energy models. All experimental data (mean ± SEM) were fitted with the 2S3B and the 3S4B models (Eqs. 3 and S8, *black* and *blue lines*, respectively). **a** *I/V* relationship in the presence of a "forward" KCl chemical gradient ($n = 4$). **b** *I/V* relationships in symmetrical K^+ (*open symbols*, $n = 4$), and in the presence of a "forward" KCl chemical gradient after addition of 135 mM LiCl to the *trans* side (*filled circles*, $n = 3$). **c** *I/V* relationship in the presence of a "reverse" KCl chemical gradient ($n = 4$). **d** *I/V* relationships in symmetrical K^+ (*open symbols*) and in the presence of a "reverse" KCl chemical gradient after addition of 135 mM LiCl to the *cis* side (*filled symbols*, $n = 4$). **e** *I/V* relationship in the presence of a LiCl chemical gradient (*filled circles*, $n = 3$). **f** Li^+/K^+ perm-selectivity ratio calculated as a ratios of the 2S3B (*black*) and 3S4B (*blue*) fits in K^+ and Li^+ "forward" condition. For comparison, the *red line* shows the perm-selectivity obtained from the GHK_o

fitting of experimental data to a Hill-type kinetic equation (Eq. 1) indicated negative cooperation between the ions within the channel pore. Departure from the single-vacancy model, particularly for Na^+ and strongly for Li^+, was further evidenced because of our failure to fit the data with a quadratic function (Fig. S2, ESM), as predicted by Schumaker and Mackinnon (1990). Thus, our observations indicate that neither the kinetic (Hill) nor the single-vacancy models completely explains PC2 channel function. Conversely, the linear response observed with Li^+ (Fig. S2) suggests single occupancy for this ion, thus masking at least one binding site, most likely because of the strong negative allosteric interaction of the high-affinity binding site (19 mM, obtained from Eq. S3, ESM). This finding is in very good agreement with the first Li^+ binding site calculated from the energy fitting (18.7 mM). Our data were better fitted with a two-exponential decay function of g/γ_i versus γ_i, noticing the weakest difference between regimes in the Li^+ data (Fig. S2, ESM). Thus, saturation binding by Li^+ even at lower concentrations is consistent with the higher affinity observed for this ion.

To better assess ionic interactions within the channel pore, energy models based on absolute rate theory of PC2 function and inhibition by Li^+ were also used. The first approximation described by Hille (1975) was the 3S4B model that fitted well our K^+ "forward" gradient data. In

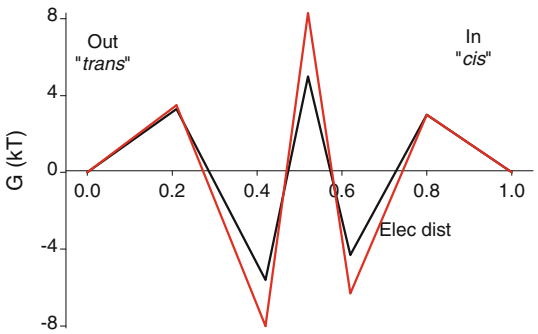

Fig. 7 Energy model of experimental data. **a** A 2S3B energy model that best fitted experimental data was constructed with fitting parameters summarized in Table S1 (mean ± SEM, *black* and *red lines* for K^+ and Li^+, respectively)

fact, the 3S4B model fitted well most experimental results despite the fact that the model does not contemplate either ion–ion interactions or multi-occupancy, which are clearly present in PC2. Further exploration with the 2S3B model rendered g closer to those obtained by GHK fits for both K^+ and Li^+ "forward" gradients. This model also fitted the "reverse" K^+ gradient and the *trans* Li^+ (bi-ionic condition). Much of the literature provides evidence that the 2S3B model accurately predicts ionic pore behaviour better than the 3S4B model for K^+, Na^+ and Ca^{2+} channels under symmetrical conditions (Almers and McCleskey 1984; Schumaker and MacKinnon 1990; French et al. 1994; Dang and McCleskey 1998). In contrast to those studies, fitting with either energy model fares much worse for conditions in the presence of electrochemical gradients, such as those in our study (Nonner et al. 1999). The fits obtained with the 2S3B model rendered the energy profile shown in Fig. 7. In this model, Li^+ displayed deeper valley energies than K^+, in agreement with the K_D obtained from the negative allosteric interaction kinetic model (Eq. S3). The model also showed a higher energy peak in the middle barrier, as predicted by Hille and Schwarz (1978), and evidenced slight asymmetry of the PC2 channel pore (Fig. 7 and also Table S1), in agreement with several of our present data.

The unexpected asymmetry of the PC2 channel was also evidenced by the shape of the *I/V* curve constructed by summation of the GHK_o fits for the "forward" and "reverse" K^+ gradients (Fig. S1a, c), which revealed a deviation from linearity with respect to the GHK_o fit in symmetrical salt (Fig. S1e, f). This evidence suggests that the asymmetry of the electrical profile in the pore is unmasked whenever chemical gradients are imposed. This is further supported by the electrostatic interactions in the 2S3B energy model. A simple exploration of the F_{in} and F_{out} ion–ion repulsion factors in Eq. S8 in the 2S3B model did not itself improve the fitting of experimental data (Figs. S3a, d). However, fitting was improved after modifying both F_{in} and the G_{12} and G_{23} energies within the channel (Fig. S3e). Thus, based on the results from calculations using Eq. S6 (ESM), it may be concluded that ion repulsion within the pore causes an increase in the affinity of the binding sites, when the first site is occupied. Ion–ion interactions can be further observed in the changes of the interaction parameter A used to describe a shift in the peak and valley energies (Alvarez et al. 1992). The distance parameters (d_1 to d_3) were also used in combination with A to calculate the energy shift of well j and peak j caused by an ion in well i (see ESM). For $A = 0.3$ obtained from several curve fits (Fig. 6), the energy shift in G_2, due to the presence of an ion in G_3, was 1.36 kT (see Table S2 for other energy shifts). To compare these findings with electrodiffusional theory, we used the fits of experimental data with the GHK equations. Subtraction of the theoretical curves obtained with the GHK_m and GHK_o equations suggested monotonic corrections for both K^+ (Fig. S1a) and Li^+ (Fig. S1b) under "forward" gradients. However, both the "reverse" K^+ gradient and the K^+–Li^+ bi-ionic

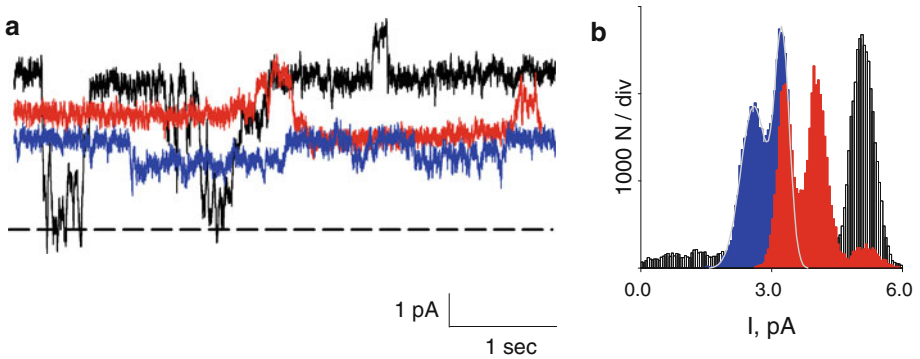

Fig. 8 Effect of low Li^+ concentrations of PC2 on single-channel currents. Representative single-channel traces of in vitro translated PC2 in the presence of a "forward" KCl chemical gradient before (*black trace*) and after addition of Li^+ 1 mM *trans* (*red trace*) and after addition of Li^+ 10 mM *trans* (*blue trace*). *Right panel* shows all-point histograms from traces on the *left*, for control (*black*), Li^+ 1 mM (*red*) and Li^+ 10 mM (*blue*) conditions, respectively ($n = 4$)

conditions suggested strong nonlinearities, likely due to electrostatic changes in the electric field inside the pore ($r > 1$, in GHK_m). Taking into consideration the voltage minima (inflection) under these two conditions (0 mV versus 11 mV, respectively, Fig. S1c–d), the energy shifts (see ESM) rendered 1.51 kT, in close agreement with that obtained from the 2S3B energy model (1.36 kT, see above). Thus, the electrical placement of the first, most external binding site shifts depending on whether K^+ or Li^+ is associated with it.

In summary, our data indicate that Li^+ permeates through, interacts with and blocks PC2 channel function. The strong Li^+ interaction, based on the energy model and K_D, indicates the much higher affinity of the ion with the pore, which explains its potential blocking effect on channel function. This is particularly interesting in light of the fact that Li^+ treatment is an important pharmacotherapy as a proven agent in bipolar disorder, in psychoses as well as diverse neurodegenerative disorders (Machado-Vieira et al. 2009). Despite the fact that the molecular mechanism of the psychopharmacological effects of Li^+ is unknown, recent studies have shown that Li^+ elongates primary cilia in a number of cultured cells (Miyoshi et al. 2009) including neurons and treated animals. Primary cilia are a chief location for PC2 expression in cells, which brings us to the effect of the low Li^+ concentration we tested. External Li^+ concentration in the range 1–10 mM reduced PC2 channel activity (Fig. 8). The presence of a functional PC2 in primary cilia whose length is affected by Li^+ suggests the possibility that this channel may be a potentially relevant clinical target. We recently postulated that ciliary length regulation may be controlled by PC2 channel activity (Li et al. 2006). Our present findings provide novel biophysical evidence for TRP channel behaviour, and suggest that Li^+ blockage of PC2 in endogenous locations such as primary cilia may help explain impairment of its sensory function and improve understanding of the biological role of Li^+ therapy.

Acknowledgments The authors are members of the Consejo Nacional de Investigaciones Científicas y Técnicas (CONICET), Argentina. The authors are deeply grateful to Dr. Patricia Bonazzola, for constant and unconditional support and encouragement, and Sumit Lal, for excellent technical support. The authors gratefully acknowledge partial support of this study by NIH ARRA award DK077079.

References

Almers W, McCleskey EW (1984) Non-selective conductance in calcium channels of frog muscle: calcium selectivity in a single-file pore. J Physiol 353:585–608

Alvarez O, Villarroel A, Eisenman G (1992) Calculation of ion currents from energy profiles and energy profiles from ion currents in multibarrier, multisite, multioccupancy channel model. Methods Enzymol 207:816–854

Bai CX, Giamarchi A, Rodat-Despoix L, Padilla F, Downs T, Tsiokas L, Delmas P (2008) Formation of a new receptor-operated channel by heteromeric assembly of TRPP2 and TRPC1 subunits. EMBO Rep 9:472–479

Cantiello HF (2003) A tale of two tails: ciliary mechanotransduction in ADPKD. Trends Mol Med 9(6):234–236

Cukierman S, Yellen G, Miller M (1985) The K^+ channel of sarcoplasmic reticulum. A new look at Cs^+ block. Biophys J 48:477–484

Dang TX, McCleskey EW (1998) Ion channel selectivity through stepwise changes in binding affinity. J Gen Physiol 111:185–1923

Delmas P (2005) Polycystins: polymodal receptor/ion-channel cellular sensors. Pflügers Arch 451(1):264–276

Eyring H, Lumry R, Woodbury JW (1949) Some applications of modern rate theory to physiological systems. Rec Chem Prog 10:100–114

French RJ, Worley JF III, Wonderlin WF, Kularatna AS, Krueger BK (1994) Ion permeation, divalent ion block, and chemical modification of single sodium channels. Description by single- and double-occupancy rate-theory models. J Gen Physiol 103(3):447–470

Glasstone S, Laidler KJ, Eyring H (1941) The theory of rate processes. McGraw-Hill, New York

González-Perrett S, Kim K, Ibarra C, Damiano AE, Zotta E, Batelli M, Harris PC, Reisin IL, Arnaout MA, Cantiello HF (2001) Polycystin-2, the protein mutated in autosomal dominant polycystic kidney disease (ADPKD), is a Ca^{2+}-permeable nonselective cation channel. Proc Natl Acad Sci USA 98(3):1182–1187

González-Perrett S, Batelli M, Kim K, Essafi M, Timpanaro G, Montalbetti N, Reisin IL M, Arnaout A, Cantiello HF (2002) Voltage dependence and pH regulation of human polycystin-2 mediated cation channel activity. J Biol Chem 277:24959–24966

Harris PC, Torres VE (2009) Polycystic kidney disease. Annu Rev Med 60:321–337

Hille B (1975) Ionic selectivity, saturation, and block in sodium channels. A four-barrier model. J Gen Physiol 66(5):535–560

Hille B (1992) Ionic channels of excitable membranes, 2nd edn. Sinauer, Sunderland

Hille B, Schwarz W (1978) Potassium channels as multi-ion single-file pores. J Gen Physiol 72(4):409–442

Hladky SB, Haydon DA (1972) Ion transfer across lipid membranes in the presence of gramicidin A. I. Studies of the unit conductance channel. Biochim Biophys Acta 274(2):294–312

Hodgkin AL, Keynes RD (1955) The potassium permeability of a giant axon nerve fiber. J Physiol 128:61–88

Ismailov II, Shlyonsky VG, Alvarez O, Benos DJ (1997) Cation permeability of a cloned rat epithelial amiloride-sensitive Na^+ channel. J Physiol 504(Pt 2):287–300

Keener J, Sneyd J (1992) Mathematical physiology, 2nd edn. Springer, Sunderland

Läuger P (1973) Ion transport through pores: a rate-theory analysis. Biochim Biophys Acta 311(3):423–441

Li Q, Montalbetti N, Wu Y, Ramos A, Raychowdhury MK, Chen XZ, Cantiello HF (2006) Polycystin-2 cation channel function is under the control of microtubular structures in primary cilia of renal epithelial cells. J Biol Chem 281(49):37566–37575

Lide DR (2009–2010) Handbook of chemistry and physics. CRC. 90th edn, pp 5–81 to 5–85

Luo Y, Vassilev PM, Li X, Kawanabe Y, Zhou J (2003) Native polycystin 2 functions as a plasma membrane Ca^{2+}-permeable cation channel in renal epithelia. Mol Cell Biol 23(7):2600–2607

Machado-Vieira R, Manji HK, Zarate CA Jr (2009) The role of lithium in the treatment of bipolar disorder: convergent evidence

for neurotrophic effects as a unifying hypothesis. Bipolar Disord 11(Suppl 2):92–109

Mackey M, McNeel M (1971) The independence principle: a reconsideration. Biophys J 11:675–680

Miyoshi K, Kasahara K, Miyazaki I, Asanuma M (2009) Lithium treatment elongates primary cilia in the mouse brain and in cultured cells. Biochem Biophys Res Commun 388(4):757–762

Mochizuki T, Wu G, Hayashi T, Xenophontos SL, Veldhuisen B, Saris JJ, Reynolds DM, Cai Y, Gabow PA, Pierides A, Kimberling WJ, Breuning MH, Deltas CC, Peters DJ, Somlo S (1996) PKD2, a gene for polycystic kidney disease that encodes an integral membrane protein. Science 272:1339–1342

Montell C (2001) Physiology, phylogeny, and functions of the TRP superfamily of cation channels. Sci STKE 90:RE1

Nauli SM, Zhou J (2004) Polycystins and mechanosensation in renal and nodal cilia. Bioessays 26(8):844–856

Nauli SM, Alenghat FJ, Luo Y, Williams E, Vassilev P, Li X, Elia AE, Lu W, Brown EM, Quinn SJ, Ingber DE, Zhou J (2003) Polycystins 1 and 2 mediate mechanosensation in the primary cilium of kidney cells. Nat Genet 33(2):129–137

Nonner W, Chen D, Eisenberg B (1999) Progress and prospects in permeation. J Gen Physiol 113:773–782

Raychowdhury MK, McLaughlin M, Ramos AJ, Montalbetti N, Bouley R, Ausiello DA, Cantiello HF (2005) Characterization of single channel currents from primary cilia of renal epithelial cells. J Biol Chem 280(41):34718–34722

Schultz SG (1980) Basic principles of membrane transport, 1st edn. Cambridge University Press, New York

Schumaker MF, MacKinnon R (1990) A simple model for multi-ion permeation. Single-vacancy conduction in a simple pore model. Biophys J 58(4):975–984

Segel IH (1975) Enzyme kinetics. Behavior and analysis of rapid equilibrium and steady state enzyme systems, Chap. 7. Wiley-Interscience, New York, pp 391–395

Timmer RT, Sands JM (1999) Lithium intoxication. J Am Soc Nephrol 10:666–674

Urban BW, Hladky SB (1979) Ion transport in the simplest single file pore. Biochim Biophys Acta 554:410–429

Urban BW, Hladky SB, Haydon DA (1978) The kinetics of ion movements in the gramicidin channel. Fed Proc 37:2628–2632

Vassilev PM, Guo L, Chen XZ, Segal Y, Peng JB, Basora N, Babakhanlou H, Cruger G, Kanazirska M, Ye CP, Brown EM, Hediger MA, Zhou J (2001) Polycystin-2 is a novel cation channel implicated in defective intracellular Ca^{2+} homeostasis in polycystic kidney disease. Biochem Biophys Res Commun 282(1):341–350

Venkatachalam K, Montell C (2007) TRP channels. Annu Rev Biochem 76:387–417. Review

Voets T, Nilius B (2003) TRP makes sense. J Membr Biol 192(1): 1–8. Review

Xu GM, González-Perrett S, Essafi M, Timpanaro GA, Montalbetti N, Arnaout MA, Cantiello HF (2003) Polycystin-1 activates and stabilizes the polycystin-2 channel. J Biol Chem 278(3):1457–1462

Zhang P, Luo Y, Chasan B, González-Perrett S, Montalbetti N, Timpanaro GA, Cantero MR, Ramos AJ, Goldmann WH, Zhou J, Cantiello HF (2009) The multimeric structure of polycystin-2 (TRPP2): structural-functional correlates of homo- and hetero-multimers with TRPC1. Hum Mol Genet 18(7):1238–1251

Zwolinski B, Eyring H, Reese C (1949) Diffusion and membrane permeability. Colloid Chem 53:1426–1453